JOURNAL OF GEOPHYSICAL RESEARCH, VOL. 97, NO. C4, PAGES 5637–5650, APRIL 15, 1992

Nonlinear Diffusion of the Tidal Signal in Frictionally Dominated Embayments

CARL T. FRIEDRICHS

Department of Geology and Geophysics, Woods Hole Oceanographic Institution, Woods Hole, Massachusetts

OLE S. MADSEN

R. M. Parsons Laboratory for Water Resources and Hydrodynamics, Department of Civil Engineering, Massachusetts Institute of Technology, Cambridge

The dynamics of many shallow tidal embayments may be usefully represented by a single "zero-inertia" equation for tidal elevation which has the form of a nonlinear diffusion equation. The zero-inertia equation clarifies the lowest order dynamics, namely, a balance between pressure gradient and friction. It also provides insight into the properties of higher-order harmonic components via the identification of compact approximate solutions and governing nondimensional parameters. Approximate analytic solutions which assume a constant diffusion coefficient are governed by the nondimensional parameters x/L and $\|k_0\|L$, where L is the length of the embayment, and $\|k_0\|^{-1}$ scales both the length of frictional dissipation and the physical length of the diffusive waveform. As $\|k_0\|L$ increases, the speed at which the tidal signal diffuses decreases, and the rate of decay of tidal amplitude with distance increases. The parameter $\|k_0\|L$ increases as depth is reduced, friction is increased, forcing amplitude or frequency is increased, or total embayment width is increased relative to the width of the channel. Approximate analytic solutions which assume a time-varying diffusion coefficient result in additional components at the zeroth, second, and third harmonic frequencies. The zeroth and second harmonics are governed by the parameter γ, as well as x/L and $\|k_0\|L$. Parameter γ measures the relative importance of time variations of channel depth ($\gamma > 0$) versus time variations in embayment width ($\gamma < 0$). If $\gamma > 0$, the diffusion coefficient is larger near the crest of the tidal waveform, causing the rising tide to be of shorter duration and mean elevation to be set up. If $\gamma < 0$, the diffusion coefficient is larger near the trough, causing the falling tide to be shorter and elevation to be set down. The third harmonic is produced by fluctuations in the diffusion coefficient associated with times of greatest surface gradient. The third harmonic is governed only by the parameters x/L and $\|k_0\|L$, which indicates the third harmonic is insensitive to time variations in cross-sectional geometry. Comparisons to field observations and to numerical solutions of the full equations including inertia terms indicate that the zero-inertia equation (1) reproduces the results of the more general one-dimensional equations to within the accuracy predicted by scaling arguments and (2) reproduces the main features of the nonlinear tidal signal observed in many shallow tidal embayments.

1. INTRODUCTION

In the study of open channel flow and flood routing, it has long been recognized that the zero-inertia approximation results in a nonlinear diffusive governing equation which advantageously can be applied to gradually varying unsteady problems [*Hayami*, 1951; *Henderson*, 1966; *Ponce et al.*, 1978]. Application of the zero-inertia approximation to flood routing leads to depth and storage dependent flood crest propagation and dissipation, and accounts for the highly asymmetric rise and fall typical of flood waves. However, it was not until recently that the zero-inertia approximation was applied to the study of nonlinear flow in tidal channels [*LeBlond*, 1978]. LeBlond showed that in shallow tidal rivers, frictional forces exceed inertial forces over most of the tidal cycle. By dropping the inertial terms in the depth-averaged one-dimensional (1-D) momentum equation, he formed a single nonlinear diffusion equation for tidal velocity and showed that long time lags associated with the propagation of low water could be accounted for by the form of the nonlinear diffusion coefficient.

Since the important work of *LeBlond* [1978], many papers have investigated nonlinearities in frictionally dominated tidal embayments using a combination of scaling arguments, field observations, and numerical modeling [*Parker*, 1984, 1991; *Aubrey and Speer*, 1985; *Speer and Aubrey*, 1985; *Friedrichs and Aubrey*, 1988; *Westerink et al.*, 1989; *Münchow and Garvine*, 1991; *Friedrichs et al.*, 1992*b*]. However, the study of tidal propagation in frictionally dominated embayments is still lacking an analytically based discussion of overtides which includes all four principal sources of nonlinearity: quadratic friction, time-varying channel depth in the friction term, and time-varying channel depth coupled with time-varying embayment width in the continuity equation. No second-order analytic study has considered the generation of harmonics by large variations in embayment width during the tidal cycle, which is the primary source of nonlinearity in many tidal embayments of interest [e.g., *Boon and Byrne*, 1981; *Friedrichs and Aubrey*, 1988]. Through analytic methods, the present paper aims to synthesize all these nonlinear mechanisms in a manner most easily adapted to physical interpretation.

Previous second-order analytic solutions to the 1-D equations with friction have been found via formal perturbation analyses [*Kreiss*, 1957; *Gallagher and Munk*, 1971; *Li*, 1974; *Kabbaj and LeProvost*, 1980; *Uncles*, 1981; *DiLorenzo*, 1988; *Shetye and Gouveia*, 1992]. Although rigorous perturbation expansions are important for spectral modeling of overtides and compound tides [*Kabbaj and LeProvost*, 1980], such techniques can make simple physical interpretation of analytical results difficult. When applied to the full 1-D equations for tidal embayments, formal perturbation

Paper number 92JC00354.
0148-0227/92/92JC-00354$05.00

analysis is algebraically intensive and results in solutions with many terms contributing to each overtide.

In this study we take a less formal approach. We make a zero-inertia assumption along the lines of *LeBlond* [1978], and form a single nonlinear diffusion equation for tidal elevation. Second-order solutions are found by approximating the nonlinear diffusion coefficient as constant in space and expanding only the time-varying portion. This approach conveniently combines the four primary nonlinear mechanisms into a single time-varying coefficient. Approximate analytic solutions for the zeroth, second, and third harmonic components are compact and allow straightforward physical interpretation via identification of their governing nondimensional parameters. Finally, we compare our approximate analytic solutions to field observations and to "exact" numerical solutions with and without the inertial terms.

In this study we examine the nonlinear properties of tidal elevation in tidal channels closed at one end. This particular application was chosen because of its relevance to a large volume of readily available field observations. Nonlinear tidal velocities in similar channels can also be examined with the 1-D zero-inertia equation. This equation may also be applied to the nonlinear properties of tidal velocity and elevation in channels with elevations forced at either end [e.g., *Wong*, 1989]. These topics are the subject of ongoing research.

1.1. *The Frictional Dominance Assumption*

Through scaling arguments, field measurement and/or numerical modeling of the individual terms in the 1-D momentum equation, many authors have demonstrated the dominance of friction over the inertial terms in well-mixed, shallow tidal embayments and estuaries. A survey of the literature (Table 1) indicates that in systems of interest (well-mixed, tidal amplitude/mean depth > ~0.1, tidal velocities ~0.5 m s^{-1}), the friction term is typically 1 to 2 orders of magnitude larger than either the local or the advective acceleration term. Furthermore, the local and advective acceleration terms are typically of opposite sign and partially cancel. In a recent paper, *Jay* [1991] showed that the local and advective acceleration terms can entirely cancel to lowest order in tidal channels with exponentially convergent geometries.

The last two entries in Table 1 serve to demonstrate the limits of the frictional dominance assumption. In the Lower Columbia River Estuary, where salinity intrusion is present, the shear stress at the bed is reduced by stratification in the water column, partially decoupling the overlying flow from the bottom [*Giese and Jay*, 1989]. Upriver beyond the intrusion of salinity, the tidal pressure gradient is primarily balanced by friction [*Giese and Jay*, 1989]. In the final example [*Pingree and Maddock*, 1978], the English Channel is simply too deep and bottom stress too small for friction to dominate the momentum equation. Approximate quantitative bounds on the conditions under which friction dominates inertia in well-mixed tidal embayments are provided by a scalar analysis of the 1-D governing equations.

The cross-sectionally integrated, 1-D equations of motion for well-mixed, channelized flow in a tidal embayment with intertidal flats (Figure 1) may be expressed as [e.g., *Speer and Aubrey*, 1985]

$$b\frac{\partial \zeta}{\partial t} + \frac{\partial (b_c h u)}{\partial x} = 0, \tag{1}$$

$$\frac{\partial u}{\partial t} + u\frac{\partial u}{\partial x} + g\frac{\partial \zeta}{\partial x} + \frac{c_d u|u|}{h} = 0, \tag{2}$$

where b is total embayment width (including tidal flats), ζ is tidal elevation, h is cross-sectionally averaged channel depth, b_c is the width of the channel, u is cross-sectionally averaged velocity (confined to the channel), and c_d is the drag coefficient. In addition to the usual assumptions of channelized flow, (1)-(2) assume $u = 0$ on the tidal flats, and $b_c/h >> 1$.

Restated in terms of characteristic scales, (1) and (2) become

$$\frac{ba}{T} + \frac{hb_c U}{L} = 0, \tag{3a}$$

$$\frac{U}{T} + \frac{U^2}{L} + \frac{ga}{L} + \frac{c_d U^2}{h} = 0, \tag{3b}$$

where a and U are the amplitudes of tidal elevation and velocity, T is the tidal period, and L is the characteristic horizontal length scale. Here we are assuming that the length scales of variation in u and ζ are of the same order. Thus this analysis is limited to nonlinearities with a basin-wide character and does not consider advective nonlinearities typically localized to smaller geometric features such as inlets, sand banks, or channel meanders [*Zimmerman*, 1978].

Solving for L in (3a) and then eliminating L in (3b) gives

$$\frac{U}{T} + \frac{baU}{b_c hT} + \frac{bga}{b_c hUT} + \frac{c_d U^2}{h} = 0. \tag{4}$$

The sum of the inertia terms is $O(U/T)$ if we assume $O(b\,a/b_c h) \le 1$. Combining the first two terms of (4) and dividing (4) by its third term gives the magnitudes of inertia and friction relative to the pressure gradient, which we assume to be order one:

$$\frac{b_c U^2 h}{ba^2 g} + 1 + \frac{b_c c_d U^3 T}{ba^2 g} = 0. \tag{5}$$

The ratio of the friction scale to the inertial scale is then

$$\frac{F}{I} = \frac{TU c_d}{h}. \tag{6}$$

In shallow tidal embayments of interest, U is of the order 0.5 m s^{-1}, $c_d \approx 10^{-2}$ - 10^{-3}, the semidiurnal period $T = 4.5 \times 10^4$ s, and 1 m $\le h \le$ 10 m. Therefore F will typically be 1 to 2 orders of magnitude larger than I in these tidally dominated embayments. Since F/I is frequency dependent, however, one should use the period of the overtide of interest when considering highly nonlinear flow. This is not a serious limitation: F will still dominate I by an order of magnitude, even if one scales (6) with the quarter-diurnal tidal period.

1.2. *Derivation of the Zero-Inertia Equation*

If we assume that frictional effects are much larger than acceleration (i.e., $F/I >> 1$), then the momentum equation for cross-sectionally averaged flow in a tidal embayment may be expressed, accurate to $O(F/I)^{-1}$, as

$$g\frac{\partial \zeta}{\partial x} + \frac{n^2 g u|u|}{h^{4/3}} = 0, \tag{7a}$$

or, equivalently,

$$u = -\frac{h^{2/3}}{n|\partial \zeta/\partial x|^{1/2}}\frac{\partial \zeta}{\partial x}, \tag{7b}$$

TABLE 1. Magnitudes of Local (LA) and Advective Acceleration (AA) Relative to the Friction Term (F), Along With Relevant Characteristic Scales

Location	LA/F	AA/F	h_0, m	a, m	U, m s^{-1}	c_d	Source
Flow through salt marsh grass	0.01	0.01	0.1	0.1	0.1	0.01	*Burke and Stolzenbach* [1983]
1-D trapezoidal channel	0.04	0.01	2	1	0.5	0.02	*Speer* [1984]
1-D model of Conwy Estuary, Wales	0.04	0.04	3	2.4	0.5	0.01	*Münchow and Garvine* [1991]
Conwy Estuary, Wales	0.05	0.02	3	2.4	0.5	0.006	*Wallis and Knight* [1984]
Fraser Estuary, BC Canada	0.05	0.05	9	4.5	1	0.005	*LeBlond* [1978]
1-D model, Stony Brk. Harbor, NY, USA	0.05	0.1	2	0.9	1	0.01	*Park* [1985]
Macquarie Harbor, Tasmania	0.1	0.007	6	0.5	1	0.004	*van de Kreeke* [1967]
Great Bay, NH USA	0.1	0.02	7	1.3	1	0.03	*Swift and Brown* [1983]
St. Lawrence Estuary, Canada	0.1	0.1	7	3.5	1	0.001	*LeBlond* [1978]
Ingram Thorofare, NJ, USA	0.2	0.07	3	0.5	0.7	0.002	*Weisman et al.* [1990]
Delaware Estuary, USA	0.4	0.03	6	0.7	1	0.0025	*Parker* [1984]
*Columbia R. Estuary, WA, USA	1	1	10	1	1	0.0008	*Giese and Jay* [1989]
*English Channel	5	2.5	40	2	0.8	0.0025	*Pingree and Maddock* [1978]

*These two examples are included to illustrate limits of the frictional dominance assumption. See text for discussion.

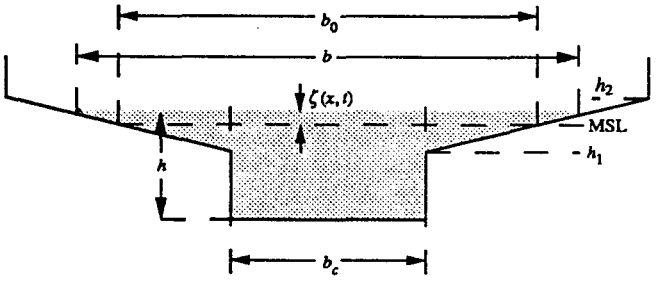

Fig. 1. Diagram of an idealized tidal embayment cross-section: $\zeta(x,t)$ is surface elevation relative to mean sea level (MSL) at the forced end of the embayment; b_c and h are the surface width and cross-sectionally averaged depth of the channel; b is the total width of the embayment cross-section, including tidal flats which act in a storage capacity only; b_0 is the time-averaged width of the embayment cross-section (at an elevation not necessarily coinciding with MSL). Elevations h_1 and h_2 are used in specifying the geometry of the intertidal storage area. Vertical exaggeration is on the order of 100:1.

where $n = h^{1/6}(c_d/g)^{1/2}$ is Manning's friction coefficient, which is assumed to be constant in space and time. (If using complex notation for ζ, the expression $|\partial\zeta/\partial x| = \mathrm{Abs}\{\mathrm{Re}(\partial\zeta/\partial x)\}$).

Inserting (7*b*) into (1) yields a single governing equation for tidal elevation in the form of a nonlinear diffusion equation:

$$\frac{\partial\zeta}{\partial t} - \frac{1}{b}\frac{\partial}{\partial x}\left\{\frac{b_c h^{5/3}}{n|\partial\zeta/\partial x|^{1/2}}\frac{\partial\zeta}{\partial x}\right\} = 0. \tag{8}$$

There are four sources of nonlinearity in (1)-(2) which contribute to the time variability of the diffusion coefficient in (8): time-varying embayment width, b, from continuity; time-varying $|\partial\zeta/\partial x|^{1/2}$ from quadratic friction; and two contributions to time-varying channel depth, namely, $h^{2/3}$ from the depth effect on friction and another power of h from continuity. Equation (8) is solved numerically in section 4, where it is compared to numerical solutions to (1)-(2), to approximate analytic solutions derived in section 3, and to field observations.

To enable approximate analytic solution, we expand the time-varying geometric parameters:

$$h^{5/3} = h_0^{5/3}\left(1 + \frac{\zeta}{h_0}\right)^{5/3} \approx h_0^{5/3}(1 + \alpha\zeta), \tag{9a}$$

$$b \approx b_0(1 + \beta\zeta), \tag{9b}$$

$$|\partial\zeta/\partial x|^{1/2} = \left(|\partial\zeta/\partial x|^{1/2}\right)_0(1 + \varepsilon(t)), \tag{9c}$$

where

$$\alpha = \frac{5}{3h_0}, \quad \beta = \frac{1}{a}\frac{\Delta b}{b_0}, \tag{9d}$$

and the dependence of ε on t will be determined in a later section. In (9) the subscript zero indicates time-averaged values, and Δb is the amplitude of change in b during the tidal cycle. Introducing (9*a*)-(9*d*) in (8) yields

$$\frac{\partial\zeta}{\partial t} - \frac{1}{b_0(1+\beta\zeta)}\frac{\partial}{\partial x}\left\{\frac{b_c h_0^{5/3}(1+\alpha\zeta)}{n\left(|\partial\zeta/\partial x|^{1/2}\right)_0(1+\varepsilon(t))}\frac{\partial\zeta}{\partial x}\right\} = 0. \tag{10}$$

In the following sections we develop approximate analytic solutions to (10). These analytic approximations allow a

straightforward interpretation of the lowest order dynamics and provide insight into the properties of higher-order harmonic components via the identification of their governing nondimensional parameters.

2. Constant Diffusion Coefficient

2.1. *Solution*

In solving the lowest order case, we neglect terms $O(\alpha\zeta,\beta\zeta,\epsilon)$ and assume b_0, b_c, h_0 and $(|\partial\zeta/\partial x|^{1/2})_0$ may be treated adequately by x-independent values. Then (10) becomes

$$\frac{\partial \zeta}{\partial t} - D_0 \frac{\partial^2 \zeta}{\partial x^2} = 0 , \tag{11}$$

where

$$D_0 = \frac{\bar{b}_c \bar{h}_0^{5/3}}{\bar{b}_0 n \overline{(|\partial\zeta/\partial x|^{1/2})}_0} = \text{constant} , \tag{12}$$

and the overbars indicate x-independent, representative values. The boundary conditions for (11) are (with the landward end at $x = 0$)

$$\zeta(x=L) = a \cos \omega t , \quad \frac{\partial \zeta}{\partial x}(x=0) = 0 . \tag{13}$$

It is not necessary to assume b_0, b_c and h_0 are x-independent to reach a first-order analytic solution. A geometric or exponential dependence on x may be treated via Bessel functions [*Prandle and Rahman*, 1980; *Friedrichs*, 1992] or by a modified Green's law approach [*Jay*, 1991]. For the embayments of interest to this study, however, the assumption of a prismatic geometry simplifies the form of the solution while retaining the essential physics.

For a linear, constant-coefficient governing equation with periodic forcing, it is convenient to employ complex variables and assume a solution of the form

$$\zeta(x,t) = \xi(x) \exp i\omega t , \tag{14}$$

where it is tacitly understood that only the real part of the complex solution is retained. If we insert (14) into (11) and solve the resulting ordinary differential equation in $\xi(x)$ subject to the boundary conditions given by (13), we have the solution

$$\zeta = a \frac{\cosh k_0 x}{\cosh k_0 L} \exp i\omega t , \tag{15}$$

where

$$k_0 = \left(\frac{i\omega}{D_0}\right)^{1/2} = (1+i)\left(\frac{\omega}{2D_0}\right)^{1/2} . \tag{16}$$

The cross-sectionally averaged velocity, u, is obtained from the continuity equation (1) as the real part of

$$u = -\frac{i\bar{b}_0 a \omega}{\bar{b}_c \bar{h}_0 k_0} \frac{\sinh k_0 x}{\cosh k_0 L} \exp i\omega t . \tag{17}$$

2.2. *Nature of the Constant Coefficient Solution*

For values of $||k_0||L << 1$ ($||k_0||$ is defined as $\{(\mathrm{Re}(k_0))^2 + (\mathrm{Im}(k_0))^2\}^{1/2}$), $\sinh k_0 x \approx k_0 x$, $\cosh k_0 L \approx 1$, and

$$\zeta \approx a \cos \omega t , \quad u \approx \frac{a\bar{b}_0 L\omega}{\bar{b}_c \bar{h}_0} \frac{x}{L} \sin \omega t , \tag{18}$$

i.e., corresponding to the simple pumping mode, with peak velocities preceding high and low water by 90°. Similarly, for $||k_0||x >> 1$, $\sinh k_0 x \approx \cosh k_0 x \approx (1/2) \exp(k_0 x)$, and

$$\begin{aligned} \zeta &\approx a \exp\left\{\frac{||k_0||}{2^{1/2}}(x-L)\right\} \cos\left\{\frac{||k_0||}{2^{1/2}}(x-L) + \omega t\right\} , \\ u &\approx \frac{a\bar{b}_0 L\omega}{\bar{b}_c \bar{h}_0 ||k_0||L} \exp\left\{\frac{||k_0||}{2^{1/2}}(x-L)\right\} \sin\left\{\frac{||k_0||}{2^{1/2}}(x-L) + \omega t - \frac{\pi}{4}\right\} , \end{aligned} \tag{19}$$

i.e., corresponding to an exponentially decaying progressive waveform traveling in the negative x direction, with peak velocities preceding high and low water by 45°. In contrast, a frictionless linear tidal wave in an infinite channel has peak velocities exactly coinciding with extreme water levels.

The nature of the frictionally dominated solution depends strongly on the channel length, L, relative to the frictional decay scale, $||k_0||^{-1} = (D_0/\omega)^{1/2}$ (Figure 2), which in turn depends on the

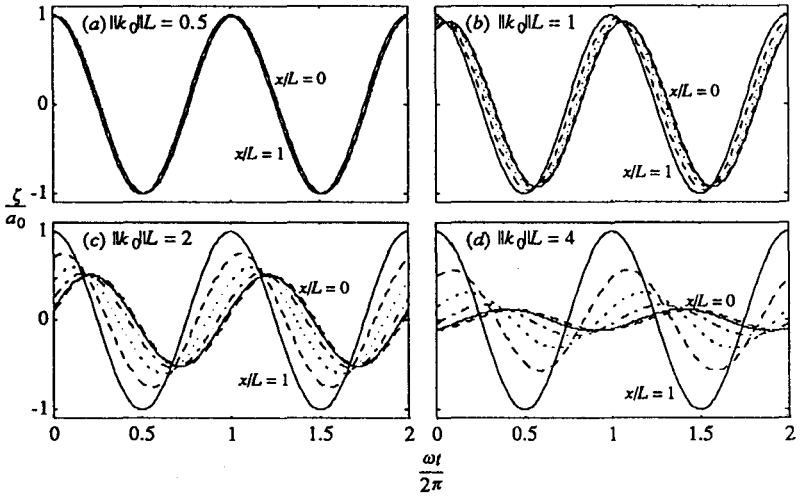

Fig. 2. Time series of (15), the analytic solution to the linearized zero-inertia equation, during two tidal cycles calculated at $x/L = 1$, 0.8, 0.6, 0.4, 0.2, and 0 ($x/L = 0$ landward): (*a*) $||k_0||L = 1/2$, (*b*) $||k_0||L = 1$, (*c*) $||k_0||L = 2$, and (*d*) $||k_0||L = 4$.

value of the diffusion coefficient given by (12). To obtain an estimate of D_0, we must evaluate the term $(|\partial\zeta/\partial x|^{1/2})_0$. From (15), the time-averaged magnitude of $\partial\zeta/\partial x$ is

$$\left|\frac{\partial\zeta}{\partial x}\right|_0 = \left\| k_0 a \frac{\sinh k_0 x}{\cosh k_0 L} \right\| \frac{2}{\pi}, \tag{20}$$

If we represent (20) with its value at $x = L$, then

$$\overline{|\partial\zeta/\partial x|_0} = \|k_0\| a \|\tanh k_0 L\| \frac{2}{\pi}. \tag{21}$$

Introducing the square root of (21) into (12), we obtain the necessary closure of the problem, i.e.,

$$D_0 = \frac{\bar{b}_c \bar{h}_0^{5/3}}{\bar{b}_0 n} \left(\|k_0\| a \|\tanh k_0 L\| \frac{2}{\pi}\right)^{-1/2}. \tag{22}$$

Since $\|k_0\| = (\omega/D_0)^{1/2}$, (22) may be written as a dispersion relationship:

$$\frac{(\|k_0\|L)^{3/2}}{(\|\tanh k_0 L\|)^{1/2}} = \frac{2^{1/2} \bar{b}_0 n a^{1/2} \omega L^{3/2}}{\pi^{1/2} \bar{b}_c \bar{h}_0^{5/3}}. \tag{23}$$

For $\|k_0\|L << 1$, $\|\tanh k_0 L\| \approx \|k_0\|L$, and (23) reduces to

$$\|k_0\|L = \left(\frac{\omega}{D_0}\right)^{1/2} L = \frac{2^{1/2} \bar{b}_0 n a^{1/2} \omega L^{3/2}}{\pi^{1/2} \bar{b}_c \bar{h}_0^{5/3}}. \tag{24}$$

For $\|k_0\|L >> 1$, $\|\tanh k_0 L\| \approx 1$, and (23) reduces to

$$\|k_0\|L = \left(\frac{\omega}{D_0}\right)^{1/2} L = \left\{\frac{2^{1/2} \bar{b}_0 n a^{1/2} \omega L^{3/2}}{\pi^{1/2} \bar{b}_c \bar{h}_0^{5/3}}\right\}^{2/3}. \tag{25}$$

According to (23)-(25), the speed at which the tidal signal diffuses decreases and the rate of decay of tidal amplitude with distance increases as channel depth is reduced, channel length is increased, friction is increased, forcing amplitude is increased, or total embayment width is increased relative to the width of the channel. Equations (23)-(25) also state that the amplitude decay rate increases as frequency is increased, indicating frictionally dominated embayments act as low-pass filters.

3. Time-Varying Diffusion Coefficient

3.1. *Governing Equation*

We now use the results from our constant coefficient solution to estimate the time dependent values of $(1 + \gamma\zeta)$, $(1 + \beta\zeta)^{-1}$, and $\{(|\partial\zeta/\partial x|^{1/2})_0 (1 + \varepsilon(t))\}^{-1}$, each of which was assumed to be constant in formulating (11). We still neglect x-dependence in these three expressions, however, and chose values at $x = L$ to be representative. Then from (15),

$$1 + \gamma\zeta \approx 1 + \gamma a \cos\omega t, \tag{26a}$$

$$(1 + \beta\zeta)^{-1} \approx (1 + \beta a \cos\omega t)^{-1} \approx 1 - \beta a \cos\omega t, \tag{26b}$$

$$\left\{\left(|\partial\zeta/\partial x|^{1/2}\right)_0 (1 + \varepsilon(t))\right\}^{-1} \approx \{\|k_0\| a \|\tanh k_0 L\| \; |\cos(\omega t + \phi + \pi/4)|\}^{-1/2}, \tag{26c}$$

where ϕ = the phase angle of $\tanh k_0 L$, and $\pi/4$ = the phase angle of k_0.

Equation (26c) may be treated more easily if we consider a Fourier series approximation of $|\cos(\omega t + \phi + \pi/4)|$ followed by the use the Binomial theorem to approximate the inverse square root:

$$|\cos(\omega t + \phi + \pi/4)| \approx \frac{2}{\pi}\left\{1 + \frac{2}{3}\cos 2(\omega t + \phi + \pi/4)\right\}, \tag{27a}$$

$$|\cos(\omega t + \phi + \pi/4)|^{-1/2} \approx \left(\frac{\pi}{2}\right)^{1/2}\left\{1 + \left(-\frac{1}{2}\right)\frac{2}{3}\cos 2(\omega t + \phi + \pi/4)\right\}. \tag{27b}$$

Figure 3*a* compares the left and right hand sides of (27*b*). From Figure 3*a* we see that the right-hand side of (27*b*) underestimates the value of $|\cos(\omega t + \phi + \pi/4)|^{-1/2}$ at the times when $|\partial\zeta/\partial x|$ is largest, i.e., precisely when we can expect discharge to be greatest and the effects of friction to be most important. Thus we will approximate $|\cos(\omega t + \phi + \pi/4)|^{-1/2}$ instead as

$$|\cos(\omega t + \phi + \pi/4)|^{-1/2} \approx \left(\frac{\pi}{2}\right)^{1/2}(1 + \delta\cos 2(\omega t + \phi + \pi/4)) \approx \left(\frac{\pi}{2}\right)^{1/2}\left(1 - \varepsilon(t)\right), \tag{28}$$

such that the minima of the two functions coincide exactly (Figure 3*b*). This gives $\delta = (2/\pi)^{1/2} - 1 \approx -0.20$. The poles indicated by Figure 3, which are poorly represented by the approximation in (28), are not significant because they coincide with slack water when friction is small.

Substituting (26) and (28) into (10) gives

$$\frac{\partial\zeta}{\partial t} - \left(\frac{\pi}{2}\right)^{1/2}\frac{1}{\bar{b}_0 n}\frac{(1 + \gamma\cos\omega t + \delta\cos(2\omega t + \theta))}{(\|k_0\| a \|\tanh k_0 L\|)^{1/2}}\frac{\partial}{\partial x}\left\{b_c h_0^{5/3}\frac{\partial\zeta}{\partial x}\right\} = 0, \tag{29a}$$

where

$$\theta = 2\phi + \frac{\pi}{2}, \tag{29b}$$

$$\gamma = a(\alpha - \beta) = \frac{5}{3}\frac{a}{h_0} - \frac{\Delta b}{b_0}. \tag{29c}$$

Relative to (8), (29) is accurate to $O(\gamma, \delta, a\alpha, a\beta)^2$ plus an unquantified error due to our choosing $x = L$ to be representative in (26). If we once again assume b_0, b_c, and h_0 to be constant in x then (29) reduces to

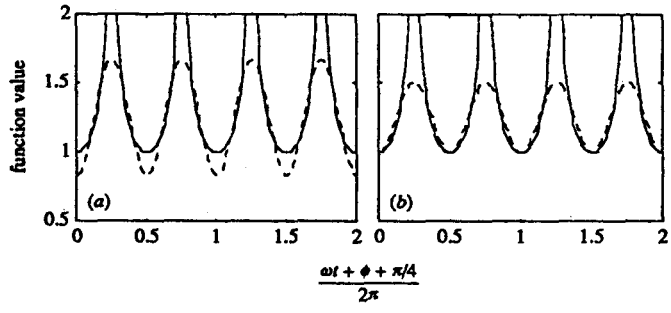

Fig. 3. Approximations of $|\cos(\omega t + \phi + \pi/4)|^{-1/2}$: (*a*) exact is solid line; $(\pi/2)^{1/2}(1 - (1/3)\cos 2(\omega t + \phi + \pi/4))$ is dashed line; (*b*) exact is solid line; $(\pi/2)^{1/2}(1 + \delta\cos 2(\omega t + \phi + \pi/4))$ is dashed line.

$$\frac{\partial \zeta}{\partial t} - \{1 + \gamma \cos \omega t + \delta \cos (2\omega t + \theta)\} D_0 \frac{\partial^2 \zeta}{\partial x^2} = 0 . \quad (30)$$

Bessel functions can be used to find approximate solutions to the higher-order harmonics in embayments with geometrically or exponentially varying along-channel geometry [*Friedrichs*, 1992]. However, the basic physics which determine the properties of the higher-order tidal components in frictionally dominated embayments are more clearly illustrated if we assume a prismatic geometry.

3.2. *Solution*

We treat the time-varying portion of the diffusion coefficient in (30) by changing variables from t to τ such that

$$\frac{\partial \zeta}{\partial t} = \frac{\partial \zeta}{\partial \tau} \frac{\partial \tau}{\partial t} = \frac{\partial \zeta}{\partial \tau} (1 + \gamma \cos \omega t + \delta \cos (2\omega t + \theta)) . \quad (31)$$

Then (31) becomes

$$\frac{\partial}{\partial \tau} \zeta(\tau,x) - D_0 \frac{\partial^2}{\partial x^2} \zeta(\tau,x) = 0 , \quad (32)$$

with

$$\omega\tau = \omega t + \gamma \sin \omega t + \frac{\delta}{2} \sin (2\omega t + \theta) . \quad (33)$$

The boundary conditions for (32) are still $\partial\zeta/\partial x = 0$ at $x = 0$, and $\zeta = a \cos \omega t$ at $x = L$. However, the boundary condition at $x = L$ must be transformed to the new time variable, τ. Utilizing (33), trigonometric identities, and approximations to $O(\gamma,\delta,a\alpha,a\beta)^2$ (for details, see *Friedrichs* [1992]), it can be shown that

$$\cos \omega t = \sum_{m=-1}^{3} A_m \cos (m\omega\tau + \varphi_m) , \quad (34)$$

where $A_{-1} = -A_3 = \delta/4$, $A_0 = -A_2 = \gamma/2$, $A_1 = 1$, $-\varphi_{-1} = \varphi_3 = \theta$, and $\varphi_0 = \varphi_1 = \varphi_2 = 0$.

Since (32) is linear, we may express the solution as a sum of terms ζ_m, each satisfying the governing equation

$$\frac{\partial \zeta_m}{\partial \tau} - D_0 \frac{\partial^2 \zeta_m}{\partial x^2} = 0 , \quad (35)$$

and the boundary conditions

$$\frac{\partial \zeta_m}{\partial x} = 0 \text{ at } x = 0, \quad \zeta_m = a A_m \cos (m\omega\tau + \varphi_m) \text{ at } x = L . \quad (36)$$

We look for solutions to (35) of the form

$$\zeta_m(x,\tau) = a A_m \xi_m(x) \exp i(m\omega\tau + \varphi_m) . \quad (37)$$

For $m \neq 1$, (37) is already $O(\gamma,\delta,a\alpha,a\beta)$, so if we discard $O(\gamma,\delta,a\alpha,a\beta)^2$ terms, (37) transforms directly back to

$$\zeta_m(x,t) = a A_m \xi_m(x) \exp i(m\omega t + \varphi_m) . \quad (38)$$

In order to transform the $m = 1$ case, we must reexpress $\exp i\omega\tau$ in terms of t. Utilizing (33), trigonometric identities, and neglecting $O(\gamma,\delta,a\alpha,a\beta)^2$ terms (for details, see *Friedrichs* [1992]), it can be shown that

$$\exp i\omega\tau = \exp i\omega t - \sum_{m \neq 1} A_m \exp i(m\omega\tau + \varphi_m) . \quad (39)$$

Equation (39) is substituted into (37) for the $m = 1$ case, and then the resulting equation is added to (38) to reconstruct the full solution in t.

We represent the full solution as a sum of single frequency components:

$$\zeta(x,t) = a \sum_{m=-1}^{3} \eta_m(x) \exp i(m\omega t + \varphi_m), \quad (40)$$

with

$$\eta_{-1} = \frac{\delta}{4} (\xi_{-1} - \xi_1) , \quad (41a)$$

$$\eta_0 = \frac{\gamma}{2} (\xi_0 - \xi_1) , \quad (41b)$$

$$\eta_1 = \xi_1 , \quad (41c)$$

$$\eta_2 = \frac{\gamma}{2} (\xi_1 - \xi_2) , \quad (41d)$$

$$\eta_3 = \frac{\delta}{4} (\xi_1 - \xi_3) . \quad (41e)$$

By substituting (37) into (35) we see that the governing equations for $\xi_m(x)$ are

$$im\omega\xi_m - D_0 \frac{d^2\xi_m}{dx^2} = 0 , \quad (42)$$

with boundary conditions

$$\frac{d\xi_m}{dx} = 0 \text{ at } x = 0, \quad \xi_m = 1 \text{ at } x = L . \quad (43)$$

Equations (42)-(43) have a solution of the same form as the constant coefficient case:

$$\xi_m = \frac{\cosh x (im\omega/D_0)^{1/2}}{\cosh L (im\omega/D_0)^{1/2}} = \frac{\cosh m^{1/2} k_0 x}{\cosh m^{1/2} k_0 L} . \quad (44)$$

3.3. *Nature of the Time-Varying Coefficient Solution*

The harmonics produced by the time-varying coefficient solution are scaled by the nondimensional parameters γ, δ, $|k_0|L$, and x/L. The parameter γ scales the zeroth harmonic, which determines set up or set down, as well as the second harmonic, which determines duration asymmetry in the rising and falling tides. If γ is positive, there is set up of mean elevation and the embayment is "shorter-rising" (Figure 4*a*). If γ is negative, there is set down and the embayment is "shorter-falling" (Figure 4*b*). These effects may be understood physically if we reexamine the definition of γ and the relevant governing equation:

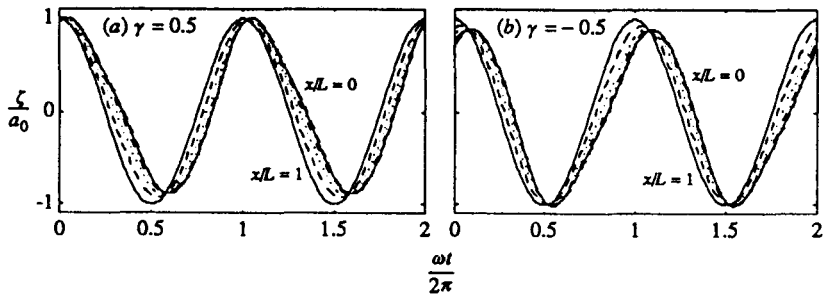

Fig. 4. Time series of (40)-(41), (44), the approximate analytic solution of the zero-inertia equation with a time-varying diffusion coefficient, with $||k_0||L = 1$ during two tidal cycles calculated at $x/L = 1, 0.8, 0.6, 0.4, 0.2$, and 0 ($x/L = 0$ landward): (*a*) $\gamma = 0.5$, and (*b*) $\gamma = -0.5$.

$$\gamma = a(\alpha - \beta) = \frac{5a}{3\bar{h}_0} - \frac{\Delta\bar{b}}{\bar{b}_0}, \tag{45}$$

$$\frac{\partial\zeta}{\partial t} - (1 + \gamma\cos\omega t + \delta\cos(2\omega t + \theta))D_0\frac{\partial^2\zeta}{\partial x^2} = 0. \tag{46}$$

If $\gamma > 0$, (45) indicates changes in channel depth during the tidal cycle are more important than changes in embayment width. (The total effect of time-varying channel depth is, in turn, 2/5 due to nonlinear friction and 3/5 due to nonlinear continuity. These proportions follow from the binomial expansion used to derive α in (9).) With $\gamma > 0$, the time-varying diffusion coefficient in (46) is larger than D_0 near the crest of the waveform ($\omega t \approx 0$), when channel depth is greatest. And the diffusion coefficient is smaller than D_0 near the trough of the waveform ($\omega t \approx \pi$), when the channel is shallowest. Since the speed at which the waveform diffuses is proportional to the square root of the diffusion coefficient, with $\gamma > 0$ the crest diffuses landward faster than the trough, "catching-up" with the trough and causing a shorter-rising asymmetry. Since the rate of decay of the waveform with distance is also proportional to the square root of the diffusion coefficient, with $\gamma > 0$ the amplitude of the crest decays more slowly than that of the trough, resulting in set up (Figure 4a).

The effect of $\gamma < 0$ is simply the opposite of $\gamma > 0$. If $\gamma < 0$, (45) indicates changes in embayment width are more important than changes in channel depth. With $\gamma < 0$, the diffusion coefficient in (46) is larger than D_0 near the trough of the waveform ($\omega t \approx \pi$), when the embayment is narrowest, and the diffusion coefficient is smaller than D_0 near the crest ($\omega t \approx 0$), when the embayment is widest. Thus with $\gamma < 0$, the trough diffuses landward faster then the crest, causing a shorter-falling asymmetry, and the trough decays more slowly than the crest, resulting in set down (Figure 4b).

With γ held constant, duration asymmetry and set up or down increase as $||k_0||L$ is increased or x/L is decreased (with $x = 0$ landward) (Figure 5). This is a straightforward consequence of the different diffusion speeds and decay rates of the crest and trough of the waveform. As $||k_0||L$ increases or x/L decreases, the effective distance over which the signals travel increases. Therefore the difference between the crest and trough travel times and the difference between the degree of crest and trough amplitude decay both increase.

These approximate analytic results are consistent with the numerical experiments of *Speer and Aubrey* [1985]. Through finite difference solutions of (1)-(2), they found that embayments with large tidal amplitude to depth ratios and small areas of intertidal flats tend to be shorter-rising, whereas embayments with small amplitude to depth ratios and large areas of intertidal flats tend to be shorter-falling. Speer and Aubrey also found tidal asymmetry to be

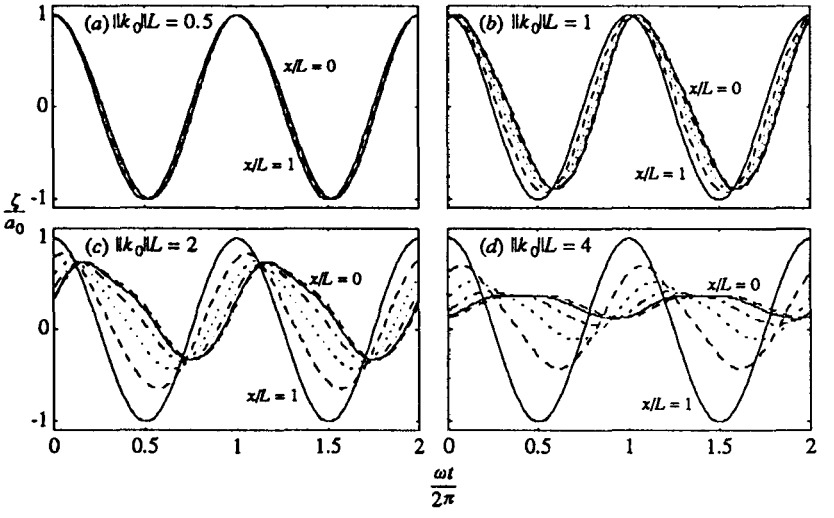

Fig. 5. Time series of (40)-(41), (44), the approximate analytic solution of the zero-inertia equation with a time-varying diffusion coefficient, with $\gamma = 0.5$ during two tidal cycles calculated at $x/L = 1, 0.8, 0.6, 0.4, 0.2$, and 0 ($x/L = 0$ landward): (*a*) $||k_0||L = 1/2$, (*b*) $||k_0||L = 1$, (*c*) $||k_0||L = 2$, and (*d*) $||k_0||L = 4$.

more sensitive to channel depth than intertidal flat extent. This latter finding is also consistent with (45), which weights $a/\bar{h}_0$ more heavily than $\Delta b/\bar{b}_0$ in the definition of γ.

The parameter δ scales the third harmonic as well as a transfer of some energy back to the first harmonic via (41a). The effect of δ in (46) can be understood if we recall that θ is ultimately related to the phase of the surface gradient. δ and θ cause the time-varying diffusion coefficient in (46) to be smaller when the surface gradient (i.e., velocity) is largest. In other words, large velocities impede the diffusion of the tidal signal.

The third harmonic does not contribute to duration asymmetries. Unlike γ, δ is not a function of cross-sectional geometry, but, to our order of approximation, δ is constant for all cross-sections. According to the approximate analytic solutions, the third harmonic varies only as a function of x/L and $|k_0|L$. Thus the third harmonic is less sensitive than the second harmonic to time variations in channel cross-section. We should expect the magnitude of the third harmonic to become progressively smaller relative to the zeroth and second harmonics as the overall tidal signal displays stronger duration asymmetry.

4. Comparison to Numerical Solutions and Observations

4.1. *Methods*

Forcing M_2 amplitude and geometric parameters required as inputs to the numerical and approximate analytic models are listed in Table 2 for 12 tidal embayments on the Atlantic Coast of the United States. The geometric parameters in Table 2 were determined by fitting the hypsometry of each embayment to an idealized, prismatic geometry with a cross-section of the form given in Figure 1. S_L is the horizontal area of the embayment that is submerged at mean low water; S_H is the area submerged at mean high water; and S_0 is the time-averaged area. Model widths were determined by averaging these areas over the length of the each real embayment. The parameter $\bar{h}_0$ is the spatially averaged depth at mean sea level of the portion of the embayment encompassed by S_L. The heights h_1 and h_2 were chosen to best represent the hypsometry of each embayment using prismatic, linearly sloping intertidal storage areas (see Figure 1).

Once prismatic approximations of the twelve real embayments were constructed, finite difference representations of (1)-(2), which include the inertia terms, were solved for each embayment. Manning's n was the only independently adjustable parameter, and it was varied until the solutions of (1)-(2) were reasonably consistent with the observed tides (Figure 6). For several of the embayments there is significant disagreement between observed and calculated M_2 phase lag (Table 3; Figure 6b), especially for small phase lags. This is largely due to the varied locations, relative to the embayment inlets, of the outside, "forcing" tide gauges needed to calculate the observed phase lags within the embayments. Set up, M_2, M_4 and M_6 were determined by least squares harmonic analyses of both the observed surface elevations and the numerical solutions to (1)-(2). Results of the harmonic analyses appear in Table 3. Also included in Table 3 are analyses of numerical solutions to (8), the governing equation without the inertia terms and approximate analytic solutions to (8) given by (40)-(41) and (44). These solutions were calculated with the same n used in the solution of (1)-(2).

The embayments at Chatham, which is shorter-rising, and North Inlet, which is shorter-falling, were examined in particular detail. These systems each contain many tide gauges and provide case studies for along-channel variation in tidal distortion.

4.2. *Numerical Solutions*

Numerical solutions to (1)-(2) and to (8), the equations of motion with and without inertia, are consistent within the scaling arguments presented in section 1.1. As predicted by (6), the two numerical solutions for M_2 disagree by about 5% or less, while amplitudes of M_4 and M_6 disagree by about 10% and 15%, respectively (Table 3; Figures 7a, 7c, and 7e). Phases predicted by the two solutions for each tidal component disagree by only a few degrees (Table 3; Figures 7b, 7d, and 7f). Disagreements between the two numerical solutions are largest for embayments with relatively deep channels (e.g., Wachapreague, Price), which is also consistent with (6). Nonetheless, these relatively small disagreements do not affect the basic dynamic balance. Thus, to the degree that the zero-inertia equation clarifies the fundamental physical balance while maintaining the most important nonlinear processes, the zero-inertia equation is a valid approximation of the more classical 1-D equations typically applied to tidally dominated shallow embayments.

The consistency of the approximate analytic solutions and the "exact" numerical results is quite good. The residuals in Figure 7 are all small in comparison to the range of the signal. Of course, there are also important differences between the analytic and numerical solutions. This is not surprising given that $a\alpha = 5a/3\bar{h}_0$ and $a\beta = \Delta b/\bar{b}_0$, which were assumed to be small, actually approach unity in several of the embayments of interest (Table 2). There are also some systematic, x-dependent differences between the numerical solutions and analytic approximations which are illustrated by a closer examination of the solutions for Chatham and North Inlet (Figure 8). Relative to the numerical results, the approximate analytic solutions for M_2 (Figures 8a-8b) tend to underestimate both amplitude decay and phase lag for large x/L (i.e., near the forced end) and overestimate them at small x/L (i.e., near the landward end). These discrepancies partly result from our treatment of $|\partial\zeta/\partial x|^{-1/2}$ in evaluating (8) analytically.

By approximating $|\partial\zeta/\partial x|^{-1/2}$ as x-independent in our analytic solution, we neglect two specific aspects of the fully nonlinear, x-dependent problem. First, we do not recover a factor of 1/2 that would appear if we were to expand (8) by differentiating an x-dependent $|\partial\zeta/\partial x|^{-1/2}$:

$$\frac{\partial}{\partial x}\left(\left|\frac{\partial\zeta}{\partial x}\right|^{-1/2}\frac{\partial\zeta}{\partial x}\right) = \operatorname{sign}\left(\frac{\partial\zeta}{\partial x}\right)\frac{\partial}{\partial x}\left(\left|\frac{\partial\zeta}{\partial x}\right|^{1/2}\right) = \frac{1}{2}\left|\frac{\partial\zeta}{\partial x}\right|^{-1/2}\frac{\partial^2\zeta}{\partial x^2} \quad (47)$$

Neglecting this differentiation overestimates the diffusion coefficient in both (11) and (46) and, therefore, underestimates the decay and delay of the tide. (We also tried differentiating $|\partial\zeta/\partial x|^{-1/2}$ before treating it as x-independent, i.e., by including the factor of 1/2. However that equally arbitrary approach caused the approximate analytic solution to be too dissipative in comparison to the numerical solutions. Hence we chose to treat $|\partial\zeta/\partial x|^{-1/2}$ as x-independent throughout the derivation.)

The second error resulting from our treatment of $|\partial\zeta/\partial x|^{-1/2}$ relates to the no-flow boundary condition, $\partial\zeta/\partial x = 0$, at $x = 0$. In (21) and (26c) we approximate $\partial\zeta/\partial x$ for all x with its nonzero value at $x = L$, therefore underestimating $|\partial\zeta/\partial x|^{-1/2}$ at small x/L (where the no-flow condition requires the surface gradient to approach zero). Since (12) indicates that the diffusion coefficient is proportional to $|\partial\zeta/\partial x|^{-1/2}$, at small x/L our approach underestimates

TABLE 2. Embayment-Wide, "Representative" Parameters Used in Calculating the Numerical and Analytic Solutions of the 1-D Governing Equations for Real Tidal Embayments

Location	L, km	$\bar{h}_0$, m	$A_{M2}(x=L)$, m	S_c, 10^6 m^2	S_0, 10^6 m^2	S_H, 10^6 m^2	h_1, m	h_2, m	$a\alpha$	$a\beta$	γ	Manning's n, m$^{-1/3}$ s	$\|k_0\|L$	Source
South Channel, Nauset, MA	8.2	1.9	0.98	2.2	3.3	4.4	-0.55	0.75	0.86	0.33	0.53	0.055	1.8	*Aubrey and Speer* [1984, 1985]; *Roman et al.* [1990]
Chatham, MA	14	2.4	1.05	18	23	28	-0.57	0.83	0.73	0.22	0.51	0.051	2.1	D. G. Aubrey, unpublished data, 1988; NOAA chart 13248
Stony Brook, NY	5.2	1.7	0.86	2.8	3.6	4.4	-0.77	0.83	0.84	0.22	0.62	0.050	1.0	USGS topo St. James; NOAA chart 12364
Shark River, NJ	4.4	1.9	0.60	2.4	3.2	4.0	-0.60	0.60	0.53	0.25	0.28	0.035	0.41	USGS topo Asbury Park
Manasquan, NJ	9.2	1.5	0.58	3.9	4.5	5.0	-0.52	0.58	0.64	0.11	0.53	0.035	1.4	USGS topo Pt. Pleasant
Wachapreague, VA	10	3.6	0.54	15	34	53	-0.55	0.55	0.25	0.56	-0.31	0.037	0.80	*Byrne et al.* [1975]; *Boon and Byrne* [1981]
Rudee, VA	1.1	4.5	0.48	0.23	0.35	0.48	-0.48	0.48	0.18	0.37	-0.19	0.040	0.01	NOAA chart 12205
Main Creek, Murrells, SC	8.0	1.9	0.73	1.6	2.6	3.6	-0.53	0.67	0.64	0.38	0.26	0.045	1.5	*Perry et al.* [1978]
Oaks Creek, Murrells, SC	4.7	1.4	0.73	0.53	1.5	2.5	-0.53	0.67	0.87	0.67	0.20	0.035	1.5	*Perry et al.* [1978]
North Inlet, SC	6.5	2.6	0.74	6.3	11	22	-0.19	0.70	0.47	1.0	-0.53	0.058	1.0	*Nummedal and Humphries* [1978]; NOAA chart 11503
Price, SC	7.1	3.3	0.69	2.7	8.8	18	-0.49	0.70	0.35	1.0	-0.70	0.030	0.74	*FitzGerald and Nummedal* [1983]; USGS topos Capers, Ft. Moultrie
Fort George, FL	8.0	2.6	0.74	4.1	5.3	6.5	-0.75	0.75	0.47	0.23	0.24	0.045	0.80	*Kojima and Hunt* [1980]; USGS topo Mayport

We define $\bar{b}_H = S_H/L$, $\bar{b}_0 = S_0/L$, $\bar{b}_c = S_c/L$, $\Delta b = \bar{b}_H - b_0$, $\alpha = 5a/3h_0$, $\beta = \Delta b/\bar{b}_0$, and $\gamma = a(\alpha - \beta)$.

TABLE 3. Observations (OB); Numerical Solutions of (1)-(2) With Inertia (NI) and of (8) the Zero-Inertia Equation (NZ); and (40)-(41), (44) the Approximate Analytic Solution of the Zero-Inertia Equation (AZ)

Location, Source	record, days	x/L	A_{M2}, m				ϕ_{M2}, deg				A_{M4}/A_{M2}				$2\phi_{M2}-\phi_{M4}$, deg				A_{M6}/A_{M2}				$3\phi_{M2}-\phi_{M6}$, deg				set up, m			
			OB	NI	NZ	AZ	OB	NI	NZ	AZ	OB	NI	NZ	AZ	OB	NI	NZ	AZ	OB	NI	NZ	AZ	OB	NI	NZ	AZ	OB	NI	NZ	AZ
South Channel, Nauset, MA																														
Aubrey and Speer [1985]	58	1	.98	.98	.98	.98	00	00	00	00	.007	.000	.000	.000	275	-----	-----	-----	.004	.000	.000	.000	180	-----	-----	-----	.000	.000	.000	.000
Aubrey and Speer [1985]	58	.86	.66	.72	.73	.80	08	19	18	14	.083	.105	.103	.027	063	067	065	035	.031	.024	.022	.008	293	354	350	227	-----	.124	.111	.048
Aubrey and Speer [1985]	29	.73	.59	.64	.65	.68	17	33	31	28	.119	.122	.122	.056	064	076	073	048	.032	.022	.020	.016	314	017	013	254	-----	.152	.135	.090
Aubrey and Speer [1985]	87	.47	.54	.60	.59	.57	29	51	48	55	.142	.134	.131	.116	064	075	074	082	.021	.026	.026	.032	339	034	030	316	-----	.156	.135	.158
Aubrey and Speer [1985]	58	.32	.57	.60	.59	.56	48	56	52	67	.142	.142	.135	.142	059	073	073	099	.023	.030	.031	.038	024	037	031	344	-----	.152	.132	.185
Aubrey and Speer [1985]	58	.12	.55	.60	.58	.56	42	59	55	76	.207	.149	.138	.160	063	073	072	111	.028	.034	.034	.043	108	040	035	006	-----	.150	.129	.206
Chatham, MA																														
Friedrichs et al. [1992*a*]	29	1	1.1	1.1	1.1	1.1	00	00	00	00	.025	.000	.000	.000	285	-----	-----	-----	.003	.000	.000	.000	215	-----	-----	-----	.000	.000	.000	.000
D. G. Aubrey, unpublished data, 1990	29	.98	.96	.97	.98	1.0	10	03	03	02	.008	.031	.029	.004	031	049	047	036	.005	.010	.009	.001	126	321	318	217	-----	.038	.034	.009
Friedrichs et al. [1992*a*]	3	.95	.80	.87	.88	.96	31	09	08	05	.033	.067	.062	.009	029	055	052	038	.015	.016	.016	.003	208	332	329	221	-----	.083	.073	.022
Friedrichs et al. [1992*a*]	29	.80	.66	.67	.69	.74	35	27	26	21	.052	.118	.115	.038	075	072	067	047	.033	.015	.016	.012	274	007	000	247	-----	.156	.137	.084
Friedrichs et al. [1992*a*]	9	.68	.66	.59	.60	.62	49	44	40	36	.074	.122	.125	.064	074	078	073	059	.049	.016	.018	.019	006	030	022	273	-----	.175	.152	.130
Friedrichs et al. [1992*a*]	29	.30	.54	.56	.54	.50	69	68	62	79	.159	.141	.133	.148	064	072	071	108	.014	.037	.038	.040	020	047	041	005	-----	.169	.145	.231
Friedrichs et al. [1992*a*]	29	0	.59	.56	.54	.50	73	71	65	90	.219	.151	.136	.169	055	071	070	124	.038	.044	.042	.046	092	050	043	032	-----	.167	.142	.257
Stony Brook, NY																														
Park [1985]	29	1	.86	.86	.86	.86	00	00	00	00	.035	.000	.000	.000	057	-----	-----	-----	-----	.000	.000	.000	-----	-----	-----	-----	.000	.000	.000	.000
Park [1985]	58	.81	.85	.79	.78	.82	28	11	11	10	.050	.075	.072	.040	041	058	058	056	-----	.009	.008	.011	-----	338	337	244	-----	.029	.028	.014
Park [1985]	58	.60	.80	.77	.76	.80	38	19	18	19	.128	.118	.111	.077	045	061	061	070	-----	.012	.010	.020	-----	348	347	267	-----	.031	.030	.028
Park [1985]	29	.21	.73	.76	.75	.79	46	25	23	29	.200	.155	.141	.117	056	064	063	085	-----	.026	.021	.031	-----	357	354	292	-----	.026	.026	.045
Shark River, NJ																														
NOS [1985]	29	.36	.60	.60	.60	.60	---	04	04	05	.018	.018	.016	.010	126	095	082	088	.035	.012	.010	.007	008	008	355	271	-----	.002	.001	.000
Manasquan, NJ																														
NOS [1985]	29	1	.58	.58	.58	.58	00	00	00	00	.012	.000	.000	.000	186	-----	-----	-----	.028	.000	.000	.000	329	-----	-----	-----	.000	.000	.000	.000
NOS [1985]	348	.35	.48	.47	.45	.45	---	40	36	45	.094	.151	.136	.124	052	058	060	085	.039	.037	.034	.034	301	006	004	309	-----	.037	.030	.064
Wachapreague, VA																														
Byrne et al. [1975]	---	1	.54	.54	.54	.54	00	00	00	00	-----	.000	.000	.000	-----	-----	-----	-----	-----	.000	.000	.000	-----	-----	-----	-----	.000	.000	.000	.000
J. D. Boon, unpublished data, 1983	347	0	.55	.55	.51	.52	19	18	15	19	.042	.063	.047	.026	203	247	236	266	.041	.057	.044	.026	337	173	160	105	-----	.022	.005	-.007
Rudee, VA																														
NOS [1985]	29	.64	.48	.48	.48	.48	---	00	00	00	.011	.000	.000	.000	193	276	267	187	.017	.000	.000	.000	087	184	176	005	-----	.000	.000	.000
Main Creek, Murrells, SC																														
NOS [1985]	58	1	.73	.73	.73	.73	00	00	00	00	.006	.000	.000	.000	047	-----	-----	-----	.005	.000	.000	.000	181	-----	-----	-----	.000	.000	.000	.000
NOS [1985]	68	.85	.59	.62	.62	.63	17	15	14	13	.100	.054	.052	.015	083	081	078	035	.030	.019	.019	.009	296	005	000	227	-----	.050	.041	.013
NOS [1985]	74	.41	.58	.56	.54	.53	30	43	39	48	.070	.086	.080	.059	098	083	082	083	.038	.040	.039	.033	343	034	030	309	-----	.069	.053	.043
NOS [1985]	106	0	.56	.56	.54	.53	45	47	43	59	.101	.094	.083	.073	091	082	081	100	.032	.046	.043	.041	002	037	032	337	-----	.068	.052	.054
Oaks Creek, Murrells, SC																														
NOS [1985]	58	1	.73	.73	.73	.73	00	00	00	00	.006	.000	.000	.000	047	-----	-----	-----	.005	.000	.000	.000	181	-----	-----	-----	.000	.000	.000	.000
NOS [1985]	100	.83	.57	.59	.60	.62	20	19	17	15	.080	.086	.078	.014	080	088	086	037	.034	.031	.029	.010	290	015	012	231	-----	.080	.063	.012
NOS [1985]	90	.38	.57	.54	.53	.52	33	43	39	50	.091	.101	.085	.048	098	099	098	085	.027	.045	.046	.034	327	051	046	313	-----	.104	.075	.036
NOS [1985]	106	0	.55	.55	.53	.53	47	46	42	60	.082	.104	.084	.057	111	099	097	100	.048	.048	.049	.041	014	053	048	338	-----	.105	.073	.043
North Inlet, SC																														
NOS [1985]	29	1	.74	.74	.74	.74	00	00	00	00	.007	.000	.000	.000	088	-----	-----	-----	.003	.000	.000	.000	086	-----	-----	-----	.000	.000	.000	.000
Nummedal and Humphries [1978]	29	.91	.64	.72	.72	.72	16	06	05	05	.043	.023	.019	.016	207	176	182	229	.009	.009	.008	.005	126	089	095	052	-.067	.012	.008	-.005
Nummedal and Humphries [1978]	29	.85	.64	.71	.71	.71	12	09	08	08	.062	.035	.030	.027	198	182	188	233	.012	.014	.012	.009	238	099	104	059	-.072	.018	.012	-.008
Eiser and Kjerfve [1986]	29	.65	.59	.70	.69	.69	---	18	16	17	.053	.067	.058	.058	190	201	205	247	.035	.027	.023	.018	248	127	129	082	-----	.031	.020	-.018
NOS [1985]	29	.46	.67	.70	.68	.68	21	22	19	24	.058	.079	.069	.081	202	209	212	257	.015	.033	.027	.025	002	139	140	099	-----	.035	.022	-.026
Eiser and Kjerfve [1986]	29	.18	.60	.70	.68	.68	---	24	22	29	.074	.087	.076	.100	225	214	217	266	.031	.038	.030	.032	025	147	146	113	-----	.038	.022	-.034
Price, SC																														
NOS [1985]	203	.84	.69	.69	.68	.68	---	06	05	05	.037	.038	.032	.025	245	222	226	248	.015	.020	.017	.007	330	137	139	071	-----	.016	.004	-.004
Ft. George, FL																														
Kojima and Hunt [1980]	2	1	.74	.74	.74	.74	00	00	00	00	.061	.000	.000	.000	312	-----	-----	-----	.038	.000	.000	.000	141	-----	-----	-----	.000	.000	.000	.000
Kojima and Hunt [1980]	2	.88	.70	.73	.72	.73	25	05	05	04	.035	.018	.015	.008	112	074	072	063	.040	.010	.009	.006	325	347	345	245	-----	.005	.004	.001
NOS [1985]	29	.35	.72	.72	.70	.71	---	15	15	15	.032	.053	.047	.027	147	079	074	079	.012	.030	.028	.019	317	002	358	272	-----	.008	.006	.005

Dashes indicate values are either unavailable or undefined.

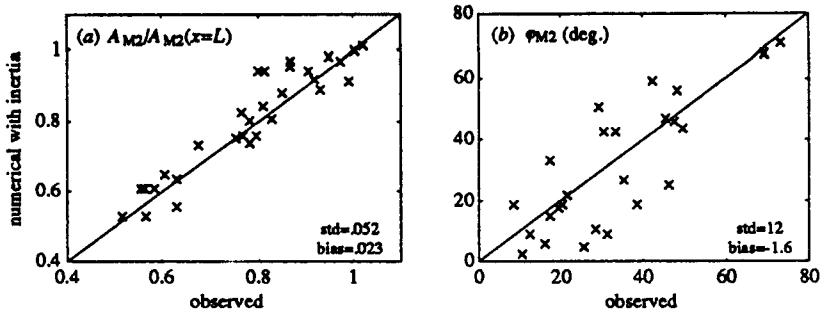

Fig. 6. Comparisons of numerical solutions to (1)-(2), the equations of motion including the inertia terms, with observations at 32 tide gauges in 12 tidal embayments (see Table 3): (*a*) M_2 amplitude divided by M_2 forcing amplitude, and (*b*) M_2 phase (deg.) relative to forcing M_2 phase. The solid line is unit slope, std is the standard deviation of the residuals from their mean, and bias is the mean residual.

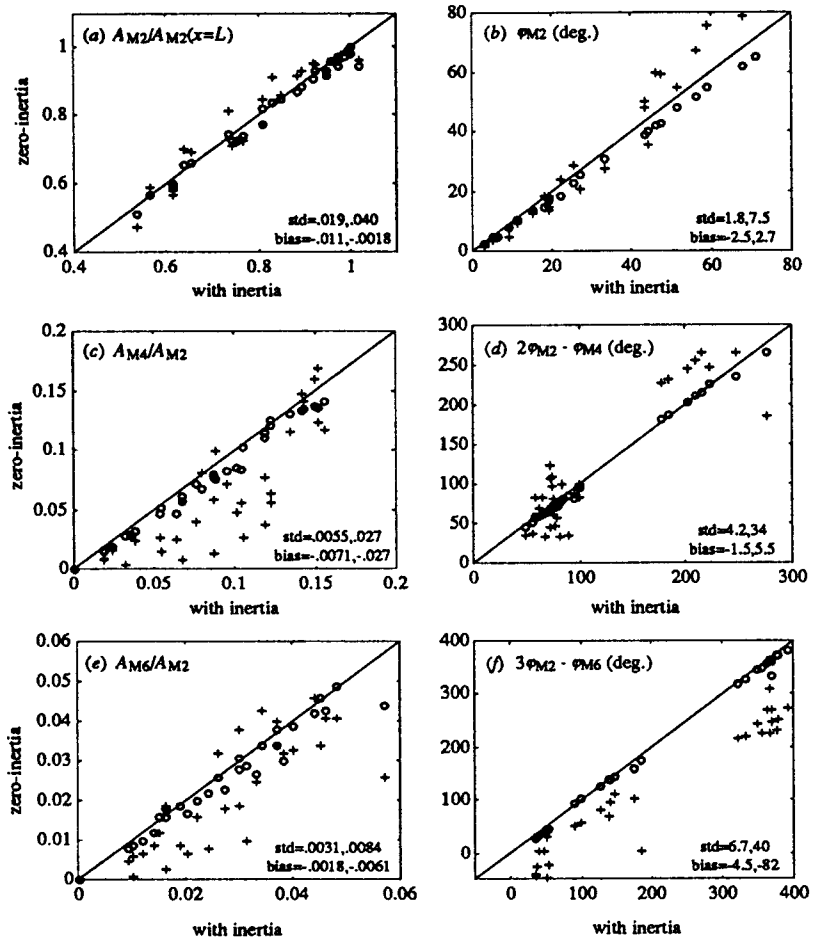

Fig. 7. Comparisons of numerical solutions to (1)-(2), the equations of motion including the acceleration terms, to numerical and approximate analytic solutions of the zero-inertia equation for 32 tide gauges in 12 tidal embayments (see Table 3): (*a*) M_2 amplitude divided by M_2 forcing amplitude, (*b*) M_2 phase (deg.) relative to forcing M_2 phase, (*c*) local M_4 to M_2 amplitude ratio, (*d*) local M_4 to M_2 relative phase (deg.), (*e*) local M_6 to M_2 amplitude ratio, and (f) local M_6 to M_2 relative phase (deg.). Numerical solution of (8), the fully nonlinear zero-inertia equation are circles; (40)-(41), (44), the approximate analytic solution with a time-varying diffusion coefficient are pluses. The solid line is unit slope, std is the standard deviation of the residuals from their mean, and bias is the mean residual.

the magnitude of the diffusion coefficient and overestimates the decay and delay of the tide. This effect, together with that described in the previous paragraph, causes the decay and delay of the tidal signal to be somewhat too small near the seaward end of the embayment and somewhat too large near the landward end. The nature of discrepancies in the higher-order harmonics is analogous. For example, the approximate analytic solutions for A_{M4}/A_{M2} (Figure 8*c*) underestimate the transfer of energy to M_4 at large x/L (cf. an underestimate of M_2 decay) and overestimate the transfer at small x/L (cf. an overestimate of M_2 decay).

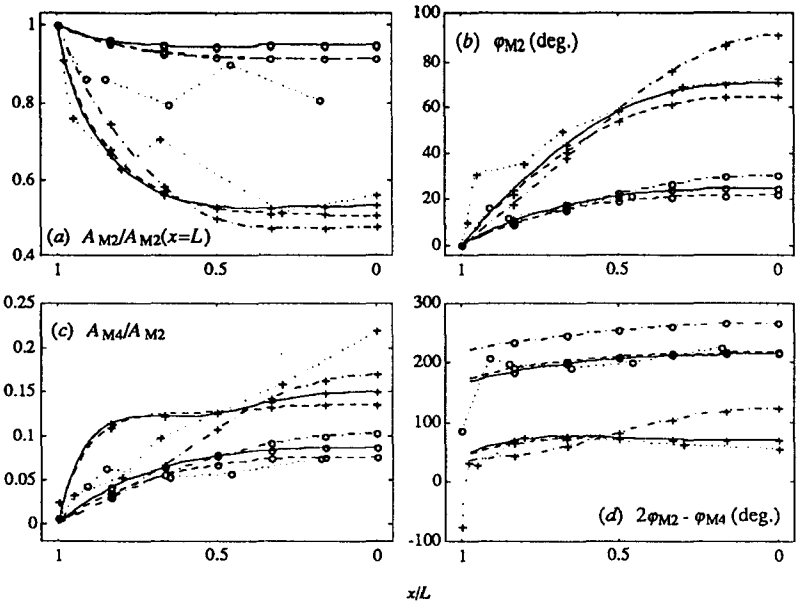

Fig. 8. Tidal surface elevation parameters as a function of distance for the tidal embayments at Chatham (pluses) and North Inlet (circles): (*a*) M_2 amplitude divided by M_2 forcing amplitude, (*b*) M_2 phase (deg.) relative to forcing M_2 phase, (*c*) local M_4 to M_2 amplitude ratio, and (*d*) local M_4 to M_2 relative phase (deg.). Field observations are dotted lines; numerical solutions to (1)-(2), which include the inertia terms, are solid lines; numerical solutions of (8), the fully nonlinear zero-inertia equation, are dashed lines; (40)-(41), (44), the approximate analytic solution with a time-varying diffusion coefficient, are dash-dot lines.

4.3. *Observations*

For the M_2 tide, the consistency of the analytic results with the observations (Figures 8*a*-8*b*, and 9*a*-9*b*) supports the overriding importance of just two nondimensional parameters, $||k_0||L$ and x/L, in determining the degree of amplitude decay and phase lag throughout frictionally dominated tidal embayments. For example, Chatham has a significantly larger value of $||k_0||L$ than North Inlet and a correspondingly larger decay and delay of the M_2 tide. In both embayments, amplitude decay and phase lag increase landward with decreased x/L. Observations are also consistent with the analytically derived roles of γ, $||k_0||L$ and x/L in determining the amplitude and relative phase of M_4 (Figures 8*c*-8*d*, 9*c*-9*d*). Chatham has a large $||k_0||L$, $\gamma > 0$, and a large M_4; North Inlet has a smaller $||k_0||L$, $\gamma < 0$, and a smaller M_4. In both embayments, A_{M4}/A_{M2} increases in magnitude landward toward $x/L = 0$. In general, all the embayments with $\gamma > 0$ are observed to be shorter-rising ($0° < 2\varphi_{M2}-\varphi_{M4} < 180°$), and all those with $\gamma < 0$ are observed to be shorter-falling ($180° < 2\varphi_{M2}-\varphi_{M4} < 360°$). Regardless of the sign of γ, observations indicate A_{M4}/A_{M2} increases as the absolute value of γ increases (Table 3).

The observed and analytic A_{M6}/A_{M2} ratios are of the same order, and both tend to increase landward (Table 3). Observed and analytic M_6 relative phases ($3\varphi_{M2}-\varphi_{M6}$) also increase as one moves landward toward $x/L = 0$. There is no discernible relationship between time variations in cross-sectional geometry and the observed M_6 tide, which is consistent with our derivation of a constant governing parameter, δ. The inability of the analytic (or numerical) results to better reproduce the observed M_6 tide may result from our treatment of Manning's n as constant in space and time. Several field studies of shallow tidal embayments suggest n can be a complex function of tidal height, flow direction, and observation location within a single embayment [e.g., *Swift and Brown*, 1983; *Wallis and Knight*, 1984; *Lewis and Lewis*, 1987].

The approximate analytic solutions and numerical results both predict significant set ups of mean tidal elevation in several of the shorter-rising embayments (Table 3). Unfortunately, none of the tidal observations for shorter-rising embayments listed in Table 2 includes references to an absolute vertical datum. However, set up has been documented in shorter-rising tidal rivers in Great Britain with tidal amplitude to depth ratios too large to be represented by the approximation $(a\alpha)^2 = (5a/3h_0)^2 << 1$ employed in this study, e.g., The Fleet [*Robinson et al.*, 1983] and the Conwy [*Wallis and Knight*, 1984], each with $(a\alpha)^2 \approx 1.8$. Observations from North Inlet do include elevation relative to an absolute datum and suggest a significant set down of the tide within North Inlet [*Nummedal and Humphries*, 1978]. Although the approximate analytic solutions to (11) do predict a small set down for North Inlet (Table 3), the numerical solutions predict a small set up. Perhaps the observed set down is due to non-tidal dynamics or an aspect of the geometry not captured in our prismatic approximation.

5. SUMMARY AND CONCLUSIONS

Scaling of the 1-D equations indicates that the friction term is typically 1 to 2 orders of magnitude larger than the inertial terms over the range of geometric and hydrodynamic parameters common to many shallow tidal embayments. Neglecting the inertial terms leads to a single "zero-inertia" governing equation for tidal elevation which has the form of a nonlinear diffusion equation. The zero-inertia equation clarifies the fundamental physical balance typical to shallow tidal embayments, while retaining the principal sources of basin-wide nonlinearity, namely, quadratic friction, time-varying channel depth, and time-varying embayment width.

First-order solutions are found by assuming the diffusion coefficient to be constant in both time and space. The first-order solutions are governed by two nondimensional parameters, $||k_0||L$ and x/L, where L is the length of the embayment, and $||k_0||^{-1}$, which is proportional to the square root of the diffusion coefficient, scales both the length of frictional dissipation and the physical length of the diffusive waveform.

As $||k_0||L$ increases, the speed at which the tidal signal diffuses

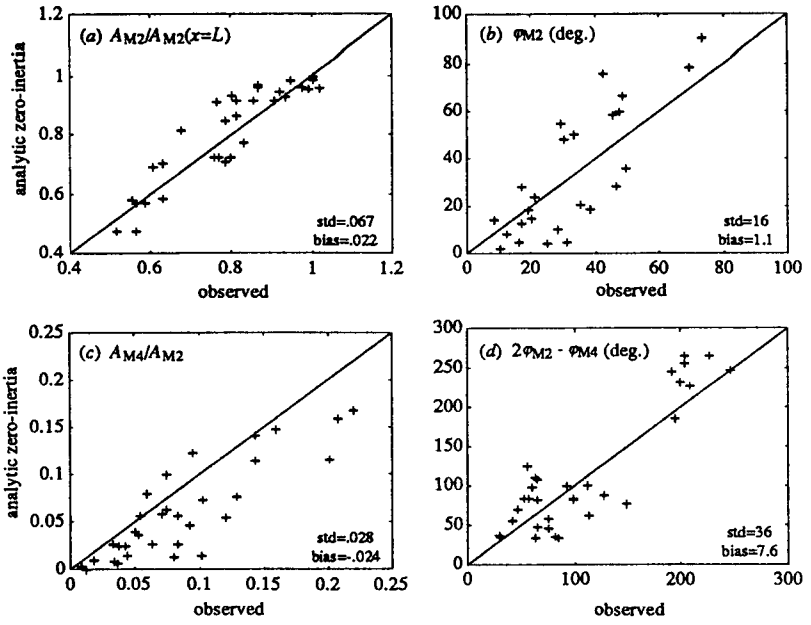

Fig. 9. Comparisons of observations at 32 tide gauges in 12 tidal embayments (see Table 3) to (40)-(41), (44), the approximate analytic solution of the zero-inertia equation with a time-varying diffusion coefficient: (*a*) M_2 amplitude divided by M_2 forcing amplitude, (*b*) M_2 phase (deg.) relative to forcing M_2 phase, (*c*) local M_4 to M_2 amplitude ratio, and (*d*) local M_4 to M_2 relative phase (deg.). The solid line is unit slope, std is the standard deviation of the residuals from their mean, and bias is the mean residual.

decreases and the rate of decay of tidal amplitude with distance increases. For $||k_0||L << 1$, the solution reduces to a simple pumping mode, whereas for $||k_0||L >> 1$, the solution reduces to an exponentially decaying, progressive waveform. $||k_0||L$ increases as depth is reduced, friction is increased, forcing amplitude or frequency is increased, or total embayment width is increased relative to the width of the channel.

Second-order solutions are found by approximating the nonlinear diffusion coefficient as constant in space and expanding only the time-varying portion. This approach conveniently combines the primary nonlinear mechanisms into a single time-varying coefficient. Approximate analytic solutions for the zeroth, second and third harmonic components are compact relative to more formal perturbation analyses and are more easily adapted to physical interpretation.

The zeroth harmonic, which determines set up or down, and the second harmonic, which determines duration asymmetry, are both governed by the parameters x/L, $||k_0||L$, and $\gamma = 5a/3h_0 - \Delta b/b_0$, where a is forcing amplitude, h_0 is average channel depth, Δb is the amplitude of time variation in embayment width, and b_0 is average embayment width.

If $\gamma > 0$, then time variations in channel depth are more important than time variations in embayment width. With $\gamma > 0$, the diffusion coefficient is larger near the crest of the waveform than near the trough. The crest diffuses landward faster and decays slower than the trough, resulting in a shorter-rising asymmetry and set up of mean elevation. If $\gamma < 0$, variations in width are more important than variations in depth. With $\gamma < 0$, the diffusion coefficient is larger near the trough of the waveform, the trough diffuses faster and decays slower, and the tide is shorter-falling and set down.

The third harmonic is produced by fluctuations in the diffusion coefficient associated with times of greatest surface gradient. The only independent parameters governing the third harmonic response are $||k_0||L$ and x/L. Thus analytic results indicate the response of the third harmonic is less geometry dependent then the response of the zeroth or second harmonics.

"Exact" numerical solutions show that the zero-inertia equation reproduces the results of the more general 1-D equations, including harmonic overtides, to within the accuracy predicted by scaling arguments for shallow tidal embayments. The approximate analytic solution to the zero-inertia equation also reproduces the main features of the numerical solutions, including the fundamental behavior of M_4 and M_6. Disagreements between analytic and numerical solutions are largely due to the neglect of space dependence in the diffusion coefficient of the analytic solution. Nonetheless, the insight provided into the numerical solutions by the analytic approximations demonstrates the usefulness of the simplified second-order approach.

Finally, observations are also consistent with the analytically derived roles of γ, $||k_0||L$ and x/L in determining the amplitude and relative phase of M_2, M_4 and M_6. Observed M_2 amplitude decay and phase lag generally increase with increased $||k_0||L$ or decreased x/L (i.e., landward). All observed embayments with with $\gamma > 0$ have shorter rising tides, and all those with $\gamma < 0$ have shorter falling tides. Observations also indicate the amplitude of M_4 generally increases as $||k_0||L$ increases, x/L decreases, or the absolute value of γ increases. The order of magnitude of the observed M_6 tide is also reproduced, but observations indicate a significant, unexplained spatial variance that is speculated to result from unresolved temporal and/or spatial variations in real embayment friction factors.

Acknowledgments. The authors would like to thank D. G. Aubrey and J. D. Boon for help in accessing data. Thanks also to J. Trowbridge for helpful comments on a draft of this manuscript. This work was supported by grants from the National Science Foundation (OCE 91-02429) and from the Ocean Ventures Fund of the Woods Hole Oceanographic Institution. WHOI contribution 7885.

REFERENCES

Aubrey, D. G., and P. E. Speer, Updrift migration of tidal inlets, *J. Geol.*, *92*, 531-545, 1984.

Aubrey, D. G., and P. E. Speer, A study of non-linear tidal propagation in shallow inlet/estuarine systems, part I: observations, *Estuarine Coastal Shelf Sci.*, *21*, 185-205, 1985.

Boon, J. D., and R. J. Byrne, On basin hypsometry and the morphodynamic response of coastal inlet systems, *Mar. Geol.*, *40*, 27-48, 1981.

Burke, R. W., and K. D. Stolzenbach, Free surface flow through salt marsh grass, *MITSG 83-16*, Massachusetts Institute of Technology Sea Grant College Program, Cambridge, 1983.

Byrne, R. J., P. Bullock, and D. G. Tyler, Response characteristics of a tidal inlet: a case study, in *Estuarine Research, Volume II: Geology and Engineering*, edited by L. E. Cronin, pp. 201-216, Academic, San Diego, Calif., 1975.

DiLorenzo, J. L., The overtide and filtering response of small inlet/bay systems, in *Hydrodynamics and Sediment Dynamics of Tidal Inlets, Coastal and Estuarine Studies*, Vol. 29, edited by D. G. Aubrey and L. Weishar, pp. 24-53, Springer-Verlag, New York, 1988.

Eiser, W. C., and B. Kjerfve, Marsh topography and hypsometric characteristics of a South Carolina salt marsh basin, *Estuarine Coastal Shelf Sci.*, *23*, 595-605, 1986.

FitzGerald, D. M., and D. Nummedal, Response characteristics of an ebb-dominated tidal inlet channel, *J. Sediment. Petrol.*, *53*, 833-845, 1983.

Friedrichs, C. T., Hydrodynamics and morphodynamics of shallow tidal channels and intertidal flats, Ph.D. Thesis, Woods Hole Oceanographic Institution - Massachusetts Institute of Technology Joint Program in Oceanography, Woods Hole, 1992.

Friedrichs, C. T., and D. G. Aubrey, Non-linear tidal distortion in shallow well-mixed estuaries: a synthesis, *Estuarine Coastal Shelf Sci.*, *27*, 521-545, 1988

Friedrichs, C. T., D. G. Aubrey, G. S. Giese, and P. E. Speer, Hydrodynamical modeling of a multiple-inlet barrier beach/estuary system: insight into tidal inlet formation and stability, in *Formation and Evolution of Multiple Inlet Systems, Coastal and Estuarine Studies*, edited by D. G. Aubrey and G. S. Giese, Springer-Verlag, New York, in press, 1992*a*.

Friedrichs, C. T., D. R. Lynch, and D. G. Aubrey, Velocity asymmetries in frictionally-dominated tidal embayments: longitudinal and lateral variability, in *Dynamics and Exchanges in Estuaries and the Coastal Zone, Coastal and Estuarine Studies*, Vol. 40, edited by D. Prandle, pp. 277-312, Springer-Verlag, New York, 1992*b*.

Gallagher, B. S., and W. H. Munk, Tides in shallow water: spectroscopy, *Tellus*, *23*, 346-363, 1971.

Giese, B. S., and D. A. Jay, Modelling tidal energetics of the Columbia River estuary, *Estuarine Coastal Shelf Sci.*, *29*, 549-571, 1989.

Hayami, S., On the propagation of flood waves, Bulletin of the Disaster Prevention Research Institute, Kyoto, Japan, 1951.

Henderson, F. M., *Open Channel Flow*, Macmillan, New York, 1966.

Jay, D. A., Green's law revisited: tidal long-wave propagation in channels with strong topography, *J. Geophys. Res.*, *96*, 20,585-20,598, 1991.

Kabbaj, A., and C. Le Provost, Nonlinear tidal waves in channels: a perturbation method adapted to the importance of quadratic bottom friction, *Tellus*, *32*, 143-163, 1980.

Kojima, H., and S. D. Hunt, Fort George Inlet, Glossary of Inlets Report 10, *FSGC Rep. 38*, University of Florida, Gainesville, 1980.

Kreiss, H., Some remarks about nonlinear oscillations in tidal channels, *Tellus*, *9*, 53-68, 1957.

LeBlond, P. H., On tidal propagation in shallow rivers, *J. Geophys. Res.*, *83*, 4717-4721, 1978.

Lewis, R. E., and J. O. Lewis, Shear stress variations in an estuary, *Estuarine Coastal Shelf Sci.*, *25*, 621-635, 1987.

Li, W.-H., Well-mixed estuaries with nonlinear resistance, *J. Hydraul. Res.*, *12*, 83-98, 1974.

Münchow, A., and R. W. Garvine, Non-linear, barotropic tides and bores in shallow estuaries, *Tellus*, *43A*, 246-256, 1991.

National Ocean Service (NOS), Index of tide stations, United States of America and miscellaneous other locations, NOAA/National Ocean Service, Rockville, Md., 1985.

Nummedal, D., and S. M. Humphries, Hydraulics and dynamics of North Inlet, 1975-76, *GITI Rep. 16*, U.S. Army Coastal Engineering Research Center, Ft. Belvoir, Va., 1978.

Park, M., Prediction of tidal hydraulics and sediment transport patterns in Stony Brook Harbor, M.S. Thesis, State University of New York, Stony Brook Marine Environmental Science Program, Stony Brook, 1985.

Parker, B. B., Frictional effects on the tidal dynamics of a shallow estuary, Ph.D. Thesis, Johns Hopkins University, Baltimore, Md., 1984.

Parker, B. B., The relative importance of the various nonlinear mechanisms in a wide range of tidal interactions (review), in *Tidal Hydrodynamics*, edited by B. B. Parker, pp. 237-268, Wiley, New York, 1991.

Perry, F. C., W. C. Seabergh, and E. F. Lane, Improvements for Murrells Inlet, South Carolina, *T.R. H-78-4*, U.S. Army Engineer Waterways Experiment Station, Vicksburg, Miss., 1978.

Pingree, R. D., and L. Maddock, The M_4 tide in the English Channel derived from a non-linear numerical model of the M_2 tide, *Deep Sea Res.*, *25*, 53-68, 1978.

Ponce, V. M., R. M. Li, and D. B. Simons, Applicability of kinematic and diffusion models, *J. Hydraul. Div., Am. Soc. Civ. Eng.*, *104 (HY3)*, 353-360, 1978.

Prandle, D., and M. Rahman, Tidal response in estuaries, *J. Phys. Oceanogr.*, *10*, 1552-1573, 1980.

Robinson, I. S., L. Warren, and J. F. Longbottom, Sea-level fluctuations in the Fleet, an English tidal lagoon, *Estuarine Coastal Shelf Sci.*, *16*, 651-668, 1983.

Roman, C. T., K. W. Able, M. A. Lazzari, and K. L. Heck, Primary productivity of angiosperm and macroalgae dominated habitats in a New England Salt Marsh: a comparative analysis, *Estuarine Coastal Shelf Sci.*, *30*, 35-45, 1990.

Shetye, S. R., and A. D. Gouveia, On the role of geometry of cross-section in generating flood-dominance in shallow estuaries, *Estuarine Coastal Shelf Sci.*, in press, 1992.

Speer, P. E., Tidal distortion in shallow estuaries, Ph.D. Thesis, Woods Hole Oceanographic Institution - Massachusetts Institute of Technology Joint Program in Oceanography, Woods Hole, 1984.

Speer, P. E., and D. G. Aubrey, A study of non-linear tidal propagation in shallow inlet/estuarine systems, part II: theory, *Estuarine Coastal Shelf Sci.*, *21*, 207-224, 1985.

Swift, M. R., and W. S. Brown, Distribution of bottom stress and tidal energy in a well-mixed estuary, *Estuarine Coastal Shelf Sci.*, *17*, 297-317, 1983.

Uncles, R. J., A note on tidal asymmetry in the Severn estuary, *Estuarine Coastal Shelf Sci.*, *13*, 419-432, 1981.

van de Kreeke, J., Water level fluctuations and flow in tidal inlets, *J. Waterw. Harbors Coastal Eng. Div., Am. Soc. Civ. Eng.*, *43 (WW2)*, 97-106, 1967.

Wallis, S. G., and D. W. Knight, Calibration studies concerning a one-dimensional numerical tidal model with particular reference to resistance coefficients, *Estuarine Coastal Shelf Sci.*, *19*, 541-562, 1984.

Weisman, R. N., G. P. Lennon, and F. E. Schuepfer, Resistence coefficient in a tidal channel, in *Estuarine and Coastal Modeling*, edited by M. L. Spaulding, pp. 123-131, American Society of Civil Engineers, New York, 1990.

Westerink, J. J., K. D. Stolzenbach, and J. J. Conner, General spectral computations of the nonlinear shallow water tidal interactions within the Bight of Abaco, *J. Phys. Oceanogr.*, *19*, 1348-1371, 1989.

Wong, K.-C., Tidally generated residual currents in a sea level canal or tidal strait with constant breadth and depth, *J. Geophys. Res.*, *94*, 8179-8192, 1989.

Zimmerman, J. T. F., Topographic generation of residual circulation by oscillatory (tidal) currents, *Geophys. Astrophys. Fluid Dyn.*, *11*, 35-47, 1978.

C. T. Friedrichs, Department of Geology and Geophysics, Woods Hole Oceanographic Institution, Woods Hole, MA 02543.

O. S. Madsen, R. M. Parsons Laboratory for Water Resources and Hydrodynamics, Department of Civil Engineering, Massachusetts Institute of Technology, Cambridge, MA 02139.

(Received November 4, 1991;
revised January 17, 1992;
accepted January 17, 1992.)